On an Exact Mapping and a Higher-Order Born Rule for Use in Analyzing Graphene Carbon Nanotubes

Dr. Michael J. Leamy
Assistant Professor
Department of Mechanical Engineering
University of Maine, Orono, ME 04469
michael.leamy@maine.edu

Dr. Peter W. Chung
Team Leader
Computational & Information Sciences Directorate
U.S. Army Research Laboratory
Aberdeen, MD 21005-5067
pchung@arl.army.mil

Dr. Raju Namburu
Branch Chief, Computational Sciences and Engineering Branch
Computational & Information Sciences Directorate
U.S. Army Research Laboratory
Aberdeen, MD 21005-5067
raju@arl.army.mil

1. Executive Summary

As part of an effort to model single-walled graphene carbon nanotubes, a transformation is first described which maps atom locations originally on a planar sheet to atom locations on a cylindrical nanotube. The mapping is parametrized by the two components describing the chiral vector, and thus is valid for generating the atomic locations of arbitrary chirality nanotubes. Attention is then turned towards quantifying the dimensions of the unit cell, again parametrized by the chiral vector's two components. Taken together, the mapping plus the unit cell dimensions are used to generate unique atomic locations of arbitrarily long carbon nanotubes.

A second mapping is described which generalizes the commonly used Born Rule to higher orders. The Born rule is an effective tool for linking bulk material deformations to atomic displacements, particularly for homogenous deformations. For non-homogenous deformations, such as those involving non-zero curvature, the standard Born Rule can inaccurately link the two scales. The higher-order mapping described herein allows non-homogenous deformations to be mapped down to the atomic scale to an arbitrary degree of precision.

The two mappings described herein are anticipated to be important developments leading to accurate deformation modeling of graphene carbon nanotubes of arbitrary chirality: the first mapping will allow for the generation of the initial atomic locations of the undeformed carbon nanotube, and the second mapping will allow subsequent deformations of the nanotube to be accurately modeled at the atomic level.

2. Introduction

The Born rule is an important component in the development of continuum models of atomic lattices. It serves as an elementary kinematic assumption that establishes a connection between atomic motion and continuum gradients, and its origins can be found in the work of Cauchy (1828,1829), who hypothesized that the gradients of the deformation agree with the motion of molecules in a deforming solid. Later, in his first book on dynamics of crystal lattices, Born generalized the hypothesis of Cauchy by allowing for the separate relaxation of internal microstructure (Born, *Dynamik der Kristallgitter*. Leipzig/Berlin: Teubner, 1915). This text was later translated into English (Born and Huang, Dynamical Theory of Crystal Lattices, Oxford: Clarendon Press, 1954). Accounting for internal relaxation has important implications for many types of crystal structures and crystal/continuum mechanics; e.g. in elastic properties of crystals in the absence or upon removal of centrosymmetry (Cousins, 1978a; Cousins 1978b; Cousins, 1979; Cousins and Martin, 1979; Cousins, 1982); in deformations involving phase transformations (Ericksen, 1984; Zanzotto, 1992; Zanzotto, 1996); in contributions to the elastic properties from n-body interactions (Martin, 1975a; Martin, 1975b; Martin, 1975c), local instabilities in the deforming Bravais lattice (Friesecke and Thiel, 2002); and in generalized schemes for transitioning atom mechanics to continuum mechanics (Friesecke and James, 2001), among others.

In general, a crystalline lattice L in its reference (unloaded) configuration is comprised of a number of interpenetrating Bravais lattices whose points are given by

$$\mathbf{X} = M^i \mathbf{a}_i + \mathbf{p}_k \,, \text{ with } i = 1, 2, 3, M^i \in Z,$$

where $\mathbf{X}$ are the lattice points, $\mathbf{a}_i$ are the linearly independent lattice vectors or Bravais base vectors, and $\mathbf{p}_k$ are the shift vectors for the inner atoms. For N+1 atoms in the basis, the index k runs from 0 to N. The base vectors $\mathbf{a}_i$ generate a so-called skeletal Bravais lattice $\mathsf{S} \subset \mathsf{L}$ where each point in S along with the k shifted atoms compose a *cluste*r, or the so-called microstructural motif (see Zanzotto, 1992). When the crystal is undeformed, the base vectors are maximal or, namely, they represent the smallest possible periodic unit of the crystal. When the

crystal is subjected to a deformation, the base vectors $\mathbf{a}_i$ are no longer maximal, in general. For this reason, let us call $\mathbf{R} = \{\mathbf{X} = M^i \mathbf{a}_i, M^i \in Z\}$ the maximal skeletal lattice of $\mathcal{L}$. Let $\mathcal{D}$ be the set of all allowable deformation gradient tensors **F** and let $\mathbf{R}'$ be the maximal skeletal lattice in the deformed configuration generated by the set of lattice vectors $\mathbf{a}'_i$. Then the formal definition of the Born rule is:

$$\mathbf{FR} = \mathbf{R}', \quad \text{i.e., } \mathbf{a}'_i = m_i^j \mathbf{F}\mathbf{a}_i \quad \text{with } \left(m_i^j\right) \in GL(3,Z), \text{ for all } \mathbf{F} \in \mathcal{D}.$$

The notation *GL(3,Z)* comes from Group Theory and refers to the classical linear group of invertible 3 by 3 matrices with integer coefficients, which effectively offers the ability to select larger sublattices that are maximal in their representation of crystal periodicity in the context of deformations.

For completeness, it is noteworthy to mention the hypothesis of Cauchy, which is more restrictive than Born's and states that for all $\mathbf{F} \in \mathcal{D}$, $\mathcal{L}$' is the deformed configuration corresponding to the undeformed $\mathcal{L}$ such that $\mathbf{F}\mathcal{L} = \mathcal{L}$'. The so-called Cauchy rule, or Cauchy-Born rule, says that the atomic motion agrees with the gross deformation of the crystal whereas the Born rule says that only the motion of the skeletal lattice agrees with the gross deformation and the microstructural motif is free to relax into its appropriate equilibrium configuration. It follows then that when the base vector of the skeletal lattice corresponds to the vector connecting nearest neighbors in a single species crystal, the Cauchy and Born hypotheses are equivalent.

In general deforming crystals, the Born rule for a maximal lattice **R** can be surprisingly restrictive despite the freedom to choose a maximal skeletal lattice in $\mathcal{L}$. In particular, and as is discussed further below, the linear nature of the rule prevents it from being applied to certain types of reduced dimension problems undergoing non-homogenous deformations, phenomena involving diffusion, lattice shuffles, or local instabilities (e.g. see Cousins and Martin, 1979; Zanzotto, 1996; Friesecke and Thiel, 2002; Arroyo and Belytschko, 2002). Another possible approach for connecting atomic motion and continuum deformations is described by Zanzotto (1992) through the so-called weak Born rule, which allows greater flexibility in the selection of the sublattices but is still subject to similar requirements as the Born rule[1].

In spite of some of its limitations, the Born rule continues to be applied in advanced computational methods with success, e.g. see Tadmor, et al. (1996) and Shilkrot, et al. (2002). In general, the rule has been found to yield excellent results in three dimensional bulk or two dimensional planar materials. The concern in this paper, however, is in its application to reduced dimensions such as thin films embedded in three dimensional space. The motivation for such problems arises naturally in contemporary problems of atomistic nanotubes and thin films, where the nanotube geometry can be constructed from a planar graphene sheet. The key issue in the modeling of such applications is the kinematic hypothesis inherent in the Born rule, which assumes that some level of homogeneity exists in the deformation map. While the concept of

[1] Our definition of the Born rule differs slightly from that of Zanzotto (1992). We presume that the Born rule pertains only to the mapping of the skeletal Bravais lattice and not to the selection of the sublattice itself. The "requirements" mentioned here are in reference to the assumptions of homogeneous deformations in the absence of instabilities, diffusion, and preservation of a Euclidean metric.

homogeneous deformation is quite standard for a three dimensional body, it is not the same for generalized geometric surfaces. These objections were noted by Arroyo and Belytschko (2002) who recognized a fundamental distinction between (1) tangents of the undeformed and deformed bodies that are mapped from one to the other via the deformation gradient **F** and (2) the chords created by lines connecting two atoms in a curved manifold. The chords are of critical importance because they determine the relative energy of an atom to its neighbor. For generalized geometric surfaces, chords are *not* mapped correctly by the deformation gradient.

Arroyo and Belytschko recognized the need to map chords correctly for generalized geometric surfaces and therefore proposed an alternative, but approximate, method to handle Born rule-like kinematics on curved manifolds using the so-called exponential Born rule. At its core is an exponential map that maps the tangent of a manifold back into the manifold itself, thereby intrinsically parameterizing the surface with the local tangents. The scheme serves as a correction step following the application of the traditional Born rule. Although effective, it requires knowledge of the surface via geodesics which, in general, involves the solution of a nonlinear system of ordinary differential equations whose unknowns are the parametric coordinates of the geodesic. For the special case of a surface that forms a uniform cylinder, the calculation is straight-forward and can be done analytically when accompanied by a geometric approximation regarding atom placement on a curved manifold (Arroyo & Belytschko, 2003). The end result is a membrane theory based only on the geodesic curvature of the cylinder, in the form of a correction that accurately maps one generalized cylindrical surface into another. It would be useful for nanotube applications to explicitly consider the nanotube chiral indices (Harris, 1999) into the mapping scheme.

In this paper, we propose an alternative method to the Born rule and exponential Born rule for general manifolds. In doing so, we explicitly consider nanotube indices for specific application to carbon nanotubes and develop the closed-form expressions for mapping an arbitrary graphene sheet into a cylindrical configuration. The larger aim is to determine the two-axis bending rigidity and torsional rigidity of a graphene carbon nanotube of arbitrary chirality. As first steps towards realizing this aim, attention is initially focused on developing a mapping for graphene sheets of arbitrary chirality which takes Bravais indices (n,m) and locates atomic positions (x,y,z) on the surface of a cylindrical carbon nanotube. In order to insure a mapping which is one-to-one, bounds on (n,m) are developed which define the domain of the so-called unit cell.

The second part of this paper details the proposed mapping, termed herein the Higher-Order Born rule, intended to replace the standard Born rule when linking bulk material deformations to atomic deformations[2]. In contrast to the Exponential Born rule, the Higher-Order Born rule eliminates the need for a correction step and is considerably quicker (in a computational sense) and easier to implement. Depending on the order to which the rule is taken, it can be used to yield a scale-linking rule of arbitrary precision.

[2] We should also note that at the time of writing, another paper (Sunyk and Steinmann, December 2003) using a higher-order gradient concept appeared that discusses the application of the Cauchy-Born rule to inhomogeneous in-plane (2D) deformations of atomistic/continuum problems. The work presented herein, however, differs in the generalization of the Born rule for arbitrary precision and its application for reduced-dimensions problems in a full three dimensional sense.

3. General Chirality Graphene Sheet to Nanotube Mapping

3.1. Mapping

In this section, a mapping $\Psi : (n,m) \in Z^2 \mapsto (x,y,z) \in R^3$ is developed taking integers *n* and *m,* indicating the usual Bravais indices for a graphene sheet, to position *(x,y,z)* on a manifold *N* representing the surface of a graphene carbon nanotube. Specifically, consider the planar graphene sheet of Fig. 1 in which $\mathbf{a}_1$ and $\mathbf{a}_2$ denote Bravais base vectors, $\mathbf{C} = N\mathbf{a}_1 + M\mathbf{a}_2$ denotes the chiral vector, $\mathbf{T} = N'\mathbf{a}_1 + M'\mathbf{a}_2$ denotes the translation vector normal to $\mathbf{C}$, and θ indicates the angle $\mathbf{C}$ makes with the reference Cartesian frame (X,Y, Z) with unit vectors $\mathbf{i}$ and $\mathbf{j}$. The length of the chiral vector can be found in any standard reference on lattice geometry,

$$C = \|\mathbf{C}\| = l_0\sqrt{N^2 + NM + M^2}\ , \tag{1}$$

where l_0 denotes the length of the basis vectors $\mathbf{a}_1$ and $\mathbf{a}_2$, which for graphene is 0.246 Å. The length of $\mathbf{T}$ determines the *unit cell*, defined to be the smallest rectangle defined by $\mathbf{C}$ and a translate of $\mathbf{C}$ such that all four corners of the unit cell coincide with an atomic lattice point. This length is also well documented, see for example (Harris, 1999), and is given by,

$$T = \|\mathbf{T}\| = l_0\sqrt{N'^2 + N'M' + M'^2} = \begin{cases} \sqrt{3}C/d_H & N - M \neq 3zd_H \\ \sqrt{3}C/(3d_H) & N - M = 3zd_H \end{cases}, \tag{2}$$

where d_H denotes the highest common divisor of *N* and *M* and *z* denotes any integer. Any lattice point on the graphene sheet can be located with a position vector **r** and lattice indices *n* and *m*, or chiral and translational coordinates *c* and *t*,

$$\mathbf{r} = n\mathbf{a}_1 + m\mathbf{a}_2 = c\mathbf{e}_c + t\mathbf{e}_t\,, \tag{3}$$

where unit vectors along $\mathbf{C}$ and $\mathbf{T}$ are denoted by $\mathbf{e}_c$ and $\mathbf{e}_t$, respectively.

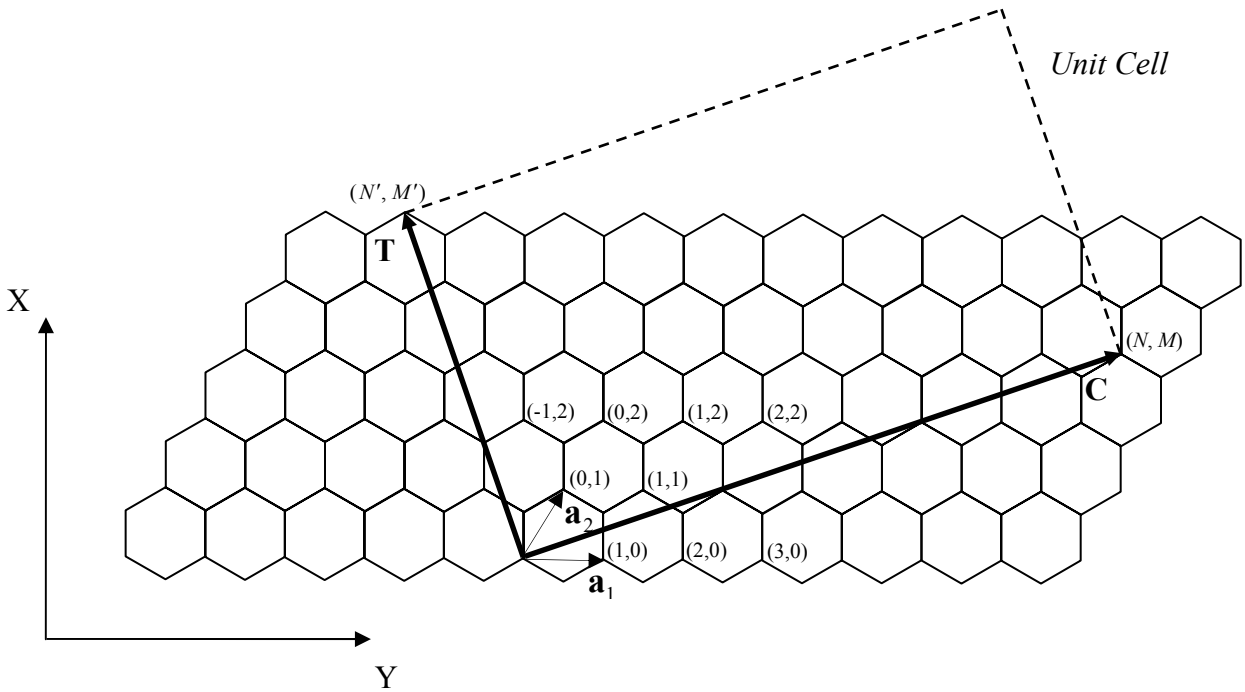

Figure 1: Lattice geometry for the graphene sheet.

Based on the above description of the graphene sheet, a mapping can be developed which describes the positions of atoms on a carbon nanotube formed by rolling-up the graphene sheet along $\mathbf{C}$, such that the two end-points of $\mathbf{C}$ occupy the same point on the nanotube, and such that $\mathbf{T}$ indicates the tubular direction. The development of this mapping starts first with the simple map Φ taking points $(X,Y,Z) \in R^3$ to $(x,y,z) \in R^3$,

$$x = \Phi_1(X,Y,Z) = r\sin(X/r),\ y = \Phi_2(X,Y,Z) = Y\ ,\ z = \Phi_3(X,Y,Z) = r\cos(X/r) - r\ , \quad (4)$$

which when applied to points on the planar manifold Π, $\Pi = \{(X,Y,0) \mid 0 \le X \le r, 0 \le Y \le l\}$, yields points on a new cylindrical manifold X with radius r and axis $\{(0,y,r) \mid 0 \le y \le l\}$, as shown in Fig. 2.

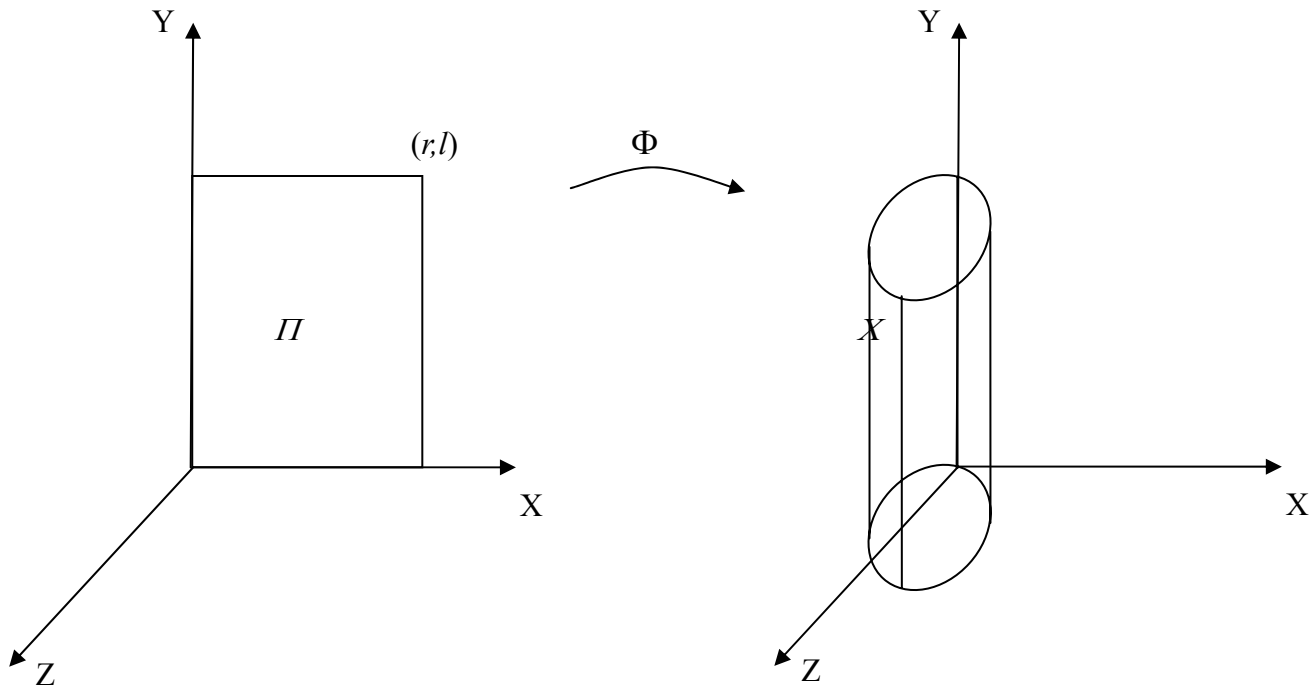

Figure 2: Mapping Φ taking planar manifold Π to cylindrical manifold X.

The mapping just described is that required to roll-up a graphene sheet along chiral vectors given by (*N*,*0*). To roll-up the sheet along any general chiral vector (*N*,*M*), Φ must be applied first to points referenced to a coordinate system aligned with the chiral and translational directions, i.e. $(c,t,Z) \in R^3$, thereby rolling up an angled sheet Π_θ (angle to the horizontal measured by θ) into an angled cylinder X_θ. Following this initial mapping, a second mapping Φ^C (corresponding to a coordinate transformation) must be applied to transform the new points on X_θ referenced to the chiral and translational axes to points referenced to the (X,Y, Z) system. The composition mapping is denoted by $\Psi^R = \Phi^C \circ \Phi : (c,t,Z) \in R^3 \mapsto (x,y,z) \in R^3$ and is given as

$$\begin{aligned} x &= \Psi_1^R(c,t,Z) = r\cos(\theta)\sin(c/r) - t\sin(\theta), \\ y &= \Psi_2^R(c,t,Z) = r\sin(\theta)\sin(c/r) + t\cos(\theta), \\ z &= \Psi_3^R(c,t,Z) = r\cos(c/r) - r, \end{aligned} \tag{5}$$

where $\Phi^C : (c,t,Z) \mapsto (x,y,z)$ is represented in matrix form by

$$\begin{Bmatrix} x \\ y \\ z \end{Bmatrix} = \begin{bmatrix} \cos\theta & -\sin\theta & 0 \\ \sin\theta & \cos\theta & 0 \\ 0 & 0 & 1 \end{bmatrix} \begin{Bmatrix} c \\ t \\ Z \end{Bmatrix}, \tag{6}$$

and where a superscript R indicates this mapping holds for points in R^3 and not in Z^2, as desired.

The desired mapping Ψ follows closely from Ψ^R. Noting that the Bravais base vectors for graphene are given as,

$$\mathbf{a}_1 = l_0\mathbf{i}, \quad \mathbf{a}_2 = \frac{1}{2}l_0\mathbf{i} + \frac{\sqrt{3}}{2}l_0\mathbf{j}, \tag{7}$$

expressions for coordinates (c,t) can be developed using (3) and (6)-(7),

$$c = l_0\frac{n+m}{2}\cos(\theta) + l_0\frac{\sqrt{3}m}{2}\sin(\theta), \quad t = -l_0\frac{n+m}{2}\sin(\theta) + l_0\frac{\sqrt{3}m}{2}\cos(\theta), \tag{8}$$

while expressions for θ and r can be developed in terms of chiral indices N and M,

$$\theta = \sin^{-1}\left(\frac{1}{2}\frac{\sqrt{3}M}{\sqrt{N^2+NM+M^2}}\right), \qquad r = \frac{1}{2}\frac{l_0\sqrt{N^2+NM+M^2}}{\pi}. \tag{9}$$

The desired map $\Psi : (n,m;N,M) \in Z^2 \mapsto (x,y,z) \in R^3$ is then arrived at after further manipulation,

$$x = \Psi_1(n,m;N,M)$$

$$= \frac{1}{4\pi}l_0\sqrt{4\left(N^2+NM+M^2\right)-3M^2}\; sin\left(\frac{\pi\left(n+\frac{m}{2}\right)\sqrt{4\left(N^2+NM+M^2\right)-3M^2}+\frac{3}{2}\pi mM}{N^2+NM+M^2}\right)$$

$$+\frac{l_0}{8}\frac{3(2n+m)M^2-3mM\sqrt{4\left(N^2+NM+M^2\right)-3M^2}}{N^2+NM+M^2},$$

$$y = \Psi_2(n,m;N,M) = \frac{1}{4\pi}l_0\sqrt{3}M\sin\left(\frac{\pi\left(n+\frac{m}{2}\right)\sqrt{4\left(N^2+NM+M^2\right)-3M^2}+\frac{3}{2}\pi mM}{N^2+NM+M^2}\right)$$

$$-\frac{l_0}{8}\frac{(2n+m)\sqrt{3}M-m\sqrt{3M}\sqrt{4\left(N^2+NM+M^2\right)-3M^2}}{N^2+NM+M^2}\sqrt{4\left(N^2+NM+M^2\right)-3M^2},$$

$$z = \Psi_3(n,m;N,M) = \frac{1}{2\pi} l_0 \sqrt{N^2 + NM + M^2} \cos\left(\frac{\pi\left(n + \frac{m}{2}\right)\sqrt{4\left(N^2 + NM + M^2\right) - 3M^2} + \frac{3}{2}\pi m M}{N^2 + NM + M^2} \right)$$

$$- \frac{l_0}{2\pi} \sqrt{N^2 + NM + M^2} \ , \tag{10}$$

where arguments after the ; indicate chiral parameters. An example of the map is shown in Fig. 3 for a (*9,5*) chiral vector.

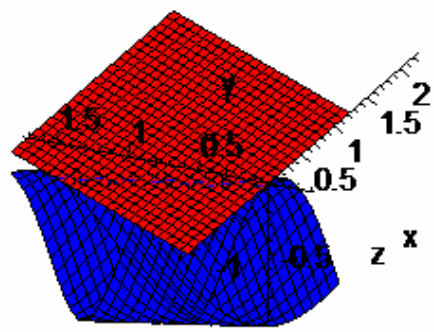

Figure 3: Cylinder (blue) generated using mapping $\Psi : (n,m;N,M) \in Z^2 \mapsto (x,y,z) \in R^3$ where (*N=9, M=5*) chirality has been chosen and where the range of indices used to generate the figure are: $-5 \le n \le 5$, $0 \le m \le 8$. The red plane indicates the locus of (X,Y,Z) locations using the given indices and before applying the map.

3.2. Unit Cell

Application of Ψ maps points from a plane to a cylinder, but without proper choice of the indices ranges for (*n,m*), results in an over-determination of the cylindrical manifold – i.e. the map is not one-to-one as more than one point on the plane is mapped to the same point on the cylinder. To prevent this occurrence, bounds on the indices are developed next which insure a domain on the plane which is mapped one-to-one onto the cylinder.

Attention is focused on the unit cell of Fig. 1 in order to develop the indices ranges. For chiral vectors with associated θ less than 60 degrees, the minimum index $m_{\min}$ for which a lattice point lies in the unit cell is 0, while the minimum index $n_{\min}$ is determined by N'. Expressions for N' and M' can be developed using the translation vector and its magnitude,

$$\mathbf{T} = T\left(-\sin\theta\,\mathbf{i} + \cos\theta\,\mathbf{j}\right) = N'\mathbf{a}_1 + M'\mathbf{a}_2 \ , \tag{11}$$

with (7). The desired expressions are,

$$n_{\min} = N' = \frac{T}{l_0}\left(-\sin\theta - \frac{1}{\sqrt{3}}\cos\theta\right), \qquad M' = \frac{2T}{\sqrt{3}l_0}\cos\theta\,. \tag{12}$$

The maximum index $n_{\max}$ is simply N, while the maximum index $m_{\max}$ is determined by the m index of a vector formed by the addition of **T** and **C** – i.e. the top-right corner of the unit cell. In order to determine this index, it is convenient to introduce the dual basis vectors $\mathbf{a}^1$ and $\mathbf{a}^2$ such that $\mathbf{a}^i \cdot \mathbf{a}_j = \delta^i{}_j$ where the center dot denotes the Cartesian inner product,

$$\mathbf{a}^1 = \frac{1}{l_0}\left(\mathbf{i} - \frac{\sqrt{3}}{3}\mathbf{j}\right), \qquad \mathbf{a}^2 = \frac{1}{l_0}\left(\frac{2\sqrt{3}}{3}\mathbf{j}\right). \tag{13}$$

Then,

$$\begin{aligned} m_{\max} &= (\mathbf{T} + \mathbf{C}) \cdot \mathbf{a}^2 \\ &= \frac{2T}{\sqrt{3}l_0}\cos\theta + M\,. \end{aligned} \tag{14}$$

Note that use of (2) and (9) in (12) and (14) yields indices bounds ($n_{\min}, n_{\max}, m_{\min}, m_{\max}$) which are only functions of the chiral vector's N and M.

With bounds identified for the indices m and n, two conditions must still be met on any pair of indices $(n_{\min} \le n \le n_{\max}, m_{\min} \le m \le m_{\max})$ to insure their existence inside of the unit cell: $0 \le c \le C$ and $0 \le t \le T$ where it is recalled that c and t are chiral and translational coordinates corresponding to (n,m) and are given by (8) while C and T are the chiral and translation vector magnitudes given by (1)-(2). Given a chiral vector (N,M), a single nested loop can be easily programmed using the minimum and maximum bounds on n and m plus the conditional checks to generate a list of index pairs of atoms located in the unit cell. The mapping Ψ given in (10) can then be applied to locate the atoms on the nanotube manifold N. Results of this procedure are shown in Fig. 4 where unit cells and nanotubes for several common chiralities are shown.

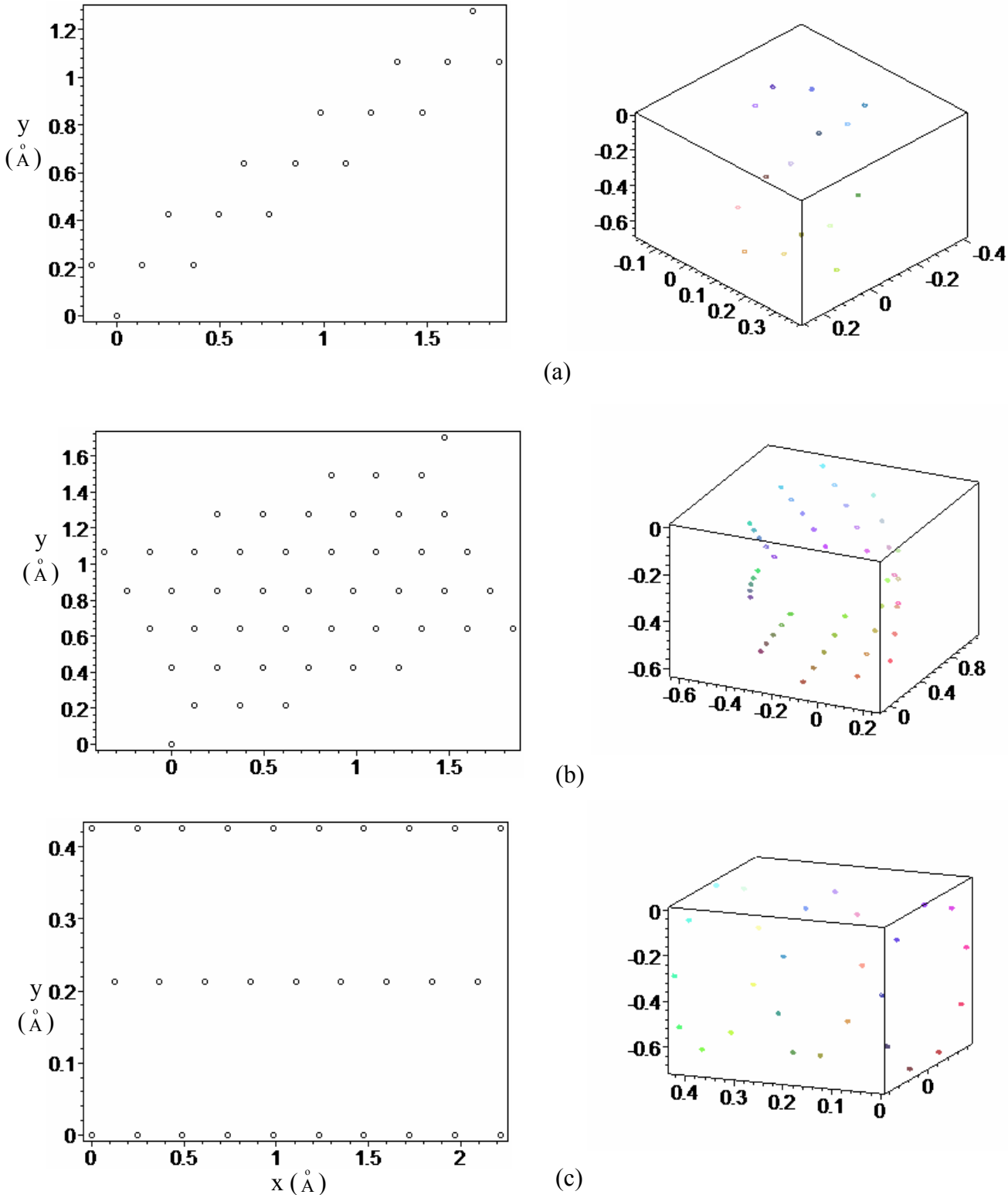

Figure 4: Results of procedure for determining the indices in the unit cell (left column) and subsequent mapping (right column) for chiral vectors (a) N=5, M=5 ; (b) N=6, M=3 ; and (c) N=9, M=0.

4. On A Higher-Order Born Rule

The Born rule is commonly employed to determine atomic lattice positions from the bulk material deformation gradient **F**. Specifically, letting $\mathbf{R}_i$ denote the a position vector of the ith atom in the continuum before deformation, and letting $\mathbf{r}_i$ denote the position of the same atom after deformation, the Born rule relates the two,

$$\mathbf{r}_i = \mathbf{F} \cdot \mathbf{R}_i \,, \tag{15}$$

where **F** referenced to Cartesian coordinates (X_1,X_2,X_3) in the undeformed configuration and (x_1,x_2,x_3) in the deformed configuration can be stated as,

$$\mathbf{F} = \frac{\partial \mathbf{r}}{\partial \mathbf{R}} = F_{iJ}\,\mathbf{e}_i \otimes \mathbf{e}_J = \frac{\partial x_i}{\partial X_J}\mathbf{e}_i \otimes \mathbf{e}_J \,. \tag{16}$$

As discussed by Arroyo and Belytschko (2002), the deformation gradient maps points on the tangent space associated with the undeformed configuration to points on the tangent space associated with the deformed configuration, and therefore inadequately maps deformations with non-zero curvature. They address this deficiency by applying the Born rule as stated in (15), and then correcting $\mathbf{r}_i$ through the exponential mapping. Note that this correction *follows* the application of the Born rule. Furthermore, by their own account, the implementation of the exponential map is "not straight forward" and requires additional simplifications. Herein, a Higher-Order Born rule is proposed which improves upon the standard Born rule by improving the *initial* mapping from $\mathbf{R}_i$ to $\mathbf{r}_i$, obviating the need for a follow-up correction, in contrast to the approach of (Arroyo and Belytschko, 2002).

As opposed to (15), the differential element **dR** maps to **dr** *exactly* through the rule

$$\mathbf{dr} = \mathbf{F} \cdot \mathbf{dR} \,, \tag{17}$$

which can be integrated once to obtain,

$$\mathbf{r} = \int \mathbf{F} \cdot \mathbf{dR} \,. \tag{18}$$

Further integration of the right-hand side requires an expression for $\mathbf{F} = \mathbf{F}(\mathbf{R})$. It is chosen to Taylor expand **F** about **R=0** without loss of generality,

$$\mathbf{F}(\mathbf{R}) = \mathbf{F}(\mathbf{0}) + \left.\frac{\partial \mathbf{F}}{\partial \mathbf{R}}\right|_{\mathbf{R}=\mathbf{0}} \cdot \mathbf{R} + O(\mathbf{R}^2) \,. \tag{19}$$

Substitution of (19) into (18) and denoting the *constant* third-order tensor $\left.\frac{\partial \mathbf{F}}{\partial \mathbf{R}}\right|_{\mathbf{R}=\mathbf{0}}$ as $\mathbf{K}$ yields the desired Higher-Order Born rule,

$$\mathbf{r} = \mathbf{F}(\mathbf{0}) \cdot \mathbf{R} + \mathbf{K} \cdot \int \mathbf{R} \cdot \mathbf{dR} + O(\mathbf{R}^2) \,. \tag{20}$$

Comparison of (20) with the standard Born rule (15) reveals the underlying assumption of the Born rule – that the deformation gradient is constant over all **R** in which it is applied. This is an adequate approximation for homogenous or small-gradient deformations like expansion, contraction, or shear, but may be inadequate for high-gradient deformations, or for bending-like deformations with non-zero curvature.

An example deformation mapping is exercised next in order to demonstrate the utility of the higher-order Born rule. Consider again the mapping Φ illustrated in Fig. 2 taking points $(X_1, X_2, X_3) \in R^3$ to $(x_1, x_2, x_3) \in R^3$,

$$\begin{aligned} x_1 = \Phi_1(X_1, X_2, X_3) = r\sin(X_1/r),\ x_2 = \Phi_2(X_1, X_2, X_3) = X_2, \\ x_3 = \Phi_3(X_1, X_2, X_3) = r\cos(X_1/r) - r\,. \end{aligned} \tag{21}$$

The deformation gradient for this map is,

$$F = \begin{bmatrix} \cos(X_1/r) & 0 & 0 \\ 0 & 1 & 0 \\ -\sin(X_1/r) & 0 & 0 \end{bmatrix}, \tag{22}$$

while the only non-zero component of $\mathbf{K}$ is $\mathrm{K}_{311} = -1/r$. Note that this indicates negative curvature in the *z-x* plane with radius of curvature *r* for all (X_1, X_2, X_3), as expected. Note further that the Higher-Order Born rule (20) for this example evaluates as,

$$\mathbf{r} = X_1\mathbf{e}_1 + X_2\mathbf{e}_2 - \frac{1}{r}\frac{X_1^{\,2}}{2}\mathbf{e}_3 + O(\mathbf{R}^2)\,, \tag{23}$$

where the non-zero $\mathbf{e}_3$ coefficient demonstrates the ability of the higher-order Born rule to more accurately map points from the plane to the cylinder. If desired, further accuracy can be obtained by taking more terms in the expansion (19). In contrast, the standard Born rule for this mapping is inadequate and would only map the plane onto itself.

5. Conclusions

Two important mappings have been developed in an effort to accomplish the larger goal of determining the two-axis bending and torsional rigidity of graphene carbon nanotubes. The first mapping allows atomic lattice coordinates to be generated for graphene carbon nanotubes of arbitrary chirality. In addition to the mapping, bounds on the Bravais indices have been developed (thereby describing a unit cell) which insure the mapping is one-to-one. The second

mapping developed allows subsequent deformations of the nanotube to be linked to atomic displacements using the newly termed Higher-Order Born rule. Although the new rule's use has been demonstrated in the context of graphene carbon nanotubes, it is expected to be equally valuable in the study of mechanics associated with any generalized geometric surface of reduced dimension which is embedded in three dimensional space.

References

Arroyo, M., Belytschko, T., 2002, "An Atomistic-Based Finite Deformation Membrane for Single Layer Crystalline Films," *Journal of the Mechanics and Physics of Solids*, V. 50, pp. 1941-1947.

Arroyo, M. and Belytschko, T., 2003, "A finite deformation membrane based on inter-atomic potentials for the transverse mechanics of nanotubes," Mechanics of Materials, 35, pp. 193—215.

Cauchy, Augustin Louis, 1828, "Sur l'équilibre et le mouvement d'un système de points matériels sollicités par des forces d'attraction ou de répulsion mutuelle," Exercices De Mathematiques. Available in Cauchy, Augustin Louis Oeuvres Complètes, Tome 20, pp. 227—252.

Cauchy, Augustin Louis, 1828, "De la pression ou tension dans un système de points matériels," Exercices De Mathematiques. Available in Cauchy, Augustin Louis Oeuvres Complètes, Tome 20, pp. 253—277.

Cauchy, Augustin Louis, 1829, "Sur les équations différentielles d'équilibre ou de movement pour un système de points matériels sollicités par des forces d'attraction ou de répulsion mutuelle," Exercices De Mathematiques. Available in Cauchy, Augustin Louis Oeuvres Complètes, Tome 21, pp. 162—173.

Cauchy, Augustin Louis, 1829, "Sur l'équilibre et le movement intérieur des corps considérés comme des masses continues," Exercices De Mathematiques. Available in Cauchy, Augustin Louis Oeuvres Complètes, Tome 21, pp. 162—173.

Cousins, CSG, 1978a, "Inner elasticity," J. Phys. C: Solid State Phys., 11, pp. 4867—4879.

Cousins, CSG, 1978b, "The symmetry of inner elastic constants," J. Phys. C: Solid State Phys., 11, pp. 4881—4900.

Cousins, CSG and Martin, JW, 1978, "Extended Cauchy discrepancies: measures of non-central, non-isotropic interactions in crystals," J. Phys. F: Metal Phys., 8(11), pp. 2279—2291.

Cousins, CSG, 1979, "General expressions for inner elastic constants," J. Phys. C: Solid State Phys., 12, pp. 1601—1607.

Cousins, CSG, 1982, "Internal strain in diamond structure elements: a survey of theoretical approaches," J. Phys. C: Solid State Phys, 15, pp. 1857—1872.

Ericksen, JL, 1984, "The Cauchy and Born hypotheses for crystals," In Phase Transformations and Material Instabilities in Solids, Proceedings of a Conference Conducted by the Mathematics Research Center, The University of Wisconsin-Madison, Orlando: Academic Press, Inc., pp. 61—77.

Friesecke, G and James, RD, 2000, "A scheme for the passage from atomic to continuum theory for thin films, nanotubes and nanorods," J. Mech. Phys. Solids, 48, 1519—1540.

Friesecke, G and Theil, F, 2002, "Validity and Failure of the Cauchy-Born Hypothesis in a Two-Dimensional Mass-Spring Lattice," Journal of Nonlinear Science, 12(5), pp. 445—478.

Harris, Peter J. F., 1999, "Carbon Nanotubes and Related Structures," *Cambridge University Press*, Cambridge, UK.

Hughes, Thomas J. R., 1987, "The Finite Element Method: Linear Static and Dynamic Finite Element Analysis," *Prentice-Hall*, New Jersey.

Martin, JW, 1975a, "Many-body forces in metals and the Brugger elastic constants," J. Phys. C: Solid State Phys., 8, pp. 2837—2857.

Martin, JW, 1975b, "Many-body forces in metals and the Brugger elastic constants: II. Inner elastic constants," J. Phys. C: Solid State Phys., 8, pp. 2858—2868.

Martin, JW, 1975c, "Many-body forces in solids: Elastic constants of diamond-type crystals," J. Phys. C: Solid State Phys., 8, pp. 2869—2888.

Shilkrot, LE, Curtin, WA, and Miller, RE, 2002, "A coupled atomistic/continuum model of defects in solids," J. Mech. Phys. Solids, 50, pp. 2085—2106.

Sunyk, R. and Steinmann, P., 2003, "On higher gradients in continuum-atomistic modeling," International Journal of Solids and Structures, 40, December, pp. 6877—6896.

Tadmor, EB, Ortiz, M, and Phillips, R, 1996, "Quasicontinuum analysis of defects in solids," Phil. Mag. A, 73(6), pp. 1529—1563.

Zanzotto, Giovanni, 1992, "On the material symmetry group of elastic crystals and the Born rule," Arch Rational Mech Anal, 121, pp. 1—36.

Zanzotto, Giovanni, 1996, "The Cauchy-Born hypothesis, nonlinear elasticity and mechanical twinning in crystals," Acta Cryst., A52, pp. 839—849.